A facile route for the synthesis of graphitic carbon-Fe-based nanocomposites from K_2CO_3-activated sugarcane bagasse

V. LORYUENYONG[a,b,*], J. PHONGTHONGCHAROEN[a], K. KLOMCHIT[a], R. CHAIKLANG[a], A. BUASRI[a,b]
aDepartment of Materials Science and Engineering, Faculty of Engineering and Industrial Technology, Silpakorn University, Nakhon Pathom 73000, Thailand
bNational Center of Excellence for Petroleum, Petrochemicals and Advanced Materials, Chulalongkorn University, Bangkok 10330, Thailand

In this study, we presented the synthesis of Fe-graphitic carbon and magnetite Fe_3O_4-amorphous carbon nanocomposites from catalytic pyrolysis and carbonization of chemically-activated sugarcane bagasse under nitrogen atmosphere. $Fe(NO_3)_3 \cdot 9H_2O$ was used as an iron precursor for preparing metallic catalyst and K_2CO_3 as an activating agent. The process was performed using a simple and low-cost chemical vapor deposition method. The obtained products were characterized by TGA, TEM, SEM, XRD, and BET specific surface area. It was observed that, at 800°C, $Fe(NO_3)_3 \cdot 9H_2O$ was decomposed and reduced to Fe_3O_4, forming magnetite Fe_3O_4-amorphous carbon nanocomposites. Graphitic carbon was, however, produced at temperatures between 900 and 1000°C, at which the iron precursor was reduced into metallic Fe nanoparticles. The BET specific surface area as high as 1159 m^2/g could be attained from the Fe/graphitic carbon nanocomposite when carbonized at 1000°C.

1. Introduction

Since the discovery of graphitic carbon nanomaterials such as fullerenes in 1985 [1] and carbon nanotubes in 1991 [2], carbon nanostructures have gained tremendous interest due to their unique morphologies and remarkable properties. Carbon nanotubes, for example, have high mechanical strength and can be either semiconducting, semimetallic, or metallic, depending upon the tube helicity and diameter [3]. Different strategies have been developed for the preparation of carbon nanotubes. The most applicable technique with large-scale favorable production is chemical vapor deposition (CVD) under an inert atmosphere and a metal catalyst (i.e., Fe, Co, Ni, Pd, etc.). This method is based on the conventional vapor-liquid-solid (VLS) mechanism, and carbon nanotubes are formed when a gaseous carbon source is decomposed over a metal catalyst [4-6].

Many commercial applications of novel graphitic carbon materials include advanced fillers, materials for energy and gas storage, sensors and components for molecular electronic devices. Recently, the applicability as adsorbent has also been extensively investigated. Previous researches have been reported that the enhancement of the adsorption capability of such materials can be performed by several techniques including oxidation treatment or the incorporation of metal oxide nanoparticles such as Fe_3O_4 [7]. Other applications involve the use of Fe_3O_4 and Fe/graphitic carbon nanocomposites for electrochemical sensing and hydrogen evolution reaction, respectively [8-9].

Nevertheless, the synthesis of graphitic carbon nanostructures or graphitic carbon-based nanocomposites relies on intensive consumption of premium chemical feedstock, energy, and costly catalysts. Therefore, it would be prudent to explore renewable and replenishable feedstock, such as those found in municipal, industrial, agricultural recycling streams. This work presents the use of resource-benign and energy-benign, cost-effective methods for the synthesis of nanocomposites based on ring-like and shell-like of graphitic nanocarbon. Sugarcane bagasse was used as a waste solid feedstock, $Fe(NO_3)_3 \cdot 9H_2O$ as a catalyst, and K_2CO_3 as a non-corrosive and environmentally friendly activating agent. Unlike other previous works, the synthesis was conducted using a simple one-furnace heating system, and a solid feedstock was chemically activated before used.

2. Experimental

2.1 Sample preparation

Sugarcane bagasse was provided by a local market in fiber form. It was first pulverized to particle sizes smaller than 500 μm using a household blender and a sieve shaker. Potassium carbonate (K_2CO_3) (Fisher Scientific Ltd.), hydrochloric acid (HCl) (Merck Millipore) and $Fe(NO_3)_3 \cdot 9H_2O$ (Ajax Finechem Pty Ltd.) were used as

purchased. The chemical activation of carbon precursor was carried out using K$_2$CO$_3$/bagasse weight ratio of 1:1.25. Fe(NO$_3$)$_3$·9H$_2$O in ethanol solution was then added into the mixture with the weight ratio of bagasse to catalyst precursor of 1:7. The mixture was introduced into a one-stage heating tube furnace (6 inches in diameter) under a flow of nitrogen carrier gas (1L/min). The furnace temperature was raised at the ramping rate of 10°C/min to different temperatures in the range of 800-1000°C and held at that temperature for 30 min. The obtained products were washed with diluted HCl solution (20 wt.%) in order to remove any metallic traces. The catalytic samples (samples labelled "800-Fe(NO$_3$)$_3$", "900-Fe(NO$_3$)$_3$", and "1000-Fe(NO$_3$)$_3$") were compared with a similar sample prepared without a catalyst and carbonized at 800°C (sample labelled "AC").

2.2 Sample characterization

XRD patterns of samples were obtained on a powder X-ray diffractometer (Rigaku, Miniflex II) with CuKα radiation having a scanning speed of 2°/s. The morphology of grown materials were examined by both scanning electron microscopy (SEM), using a Camscan MX2000 and transmission electron microscopy (TEM), using a JEOL JEM-1230. The thermogravimetric analysis (TGA) measurements were carried out in oxygen atmosphere at the heating rate of 10°C/min using Perkin Elmer TGA7HT. Fourier transform (FT-IR) measurements were performed using Bruker Optics, Vertex70. The specific surface area and pore size were measured by nitrogen adsorption/desorption at 77 K (Quantachrome, Autosorb-iQ) using BET and BJH methods.

3. Results and discussion

Thermogravimetric analysis in oxygen atmosphere is applied to assess the carbon components contained in the products. It is observed that the samples experience a major two-step weight reduction (Fig. 1). The weight of the samples first decreases rapidly at around 250°C. This weight loss is attributed to the oxidation of amorphous carbon. As the temperature increases further to 500-600°C, the samples experience additional weight loss due to the oxidation of graphitic carbon. These TGA results indicate the presence of more than one carbon structures in the samples. After 600°C, the profiles plateau to some constant weight level, representing the remaining of noncombustible metallic catalyst residues. Lorentizian functions are fitted to DTA curves in order to calculate the under curve area of each peak. The results, not shown here, indicate that the yield of graphitic carbon is optimized at the carbonization temperature of 900°C.

FT-IR spectra (Fig. 2) are measured in the range of 4000 – 400 cm^{-1}. All of the spectra show a strong broad band at 3450 cm^{-1} and a peak at 1636 cm^{-1} which are assigned to the stretching and bending modes of O-H group, respectively. The peak superimposed on the tail of

–OH bending peak at 1600 cm^{-1} can be identified as a C=C bond in aromatic ring, which is a building block of hexagonal graphitic carbon network. There is also an absorption peak at 1380 cm^{-1} due to the C-OH bending vibration. It is noticed that, at 800°C (line b), two absorption bands centered at 580 cm^{-1} and 990 cm^{-1} are significantly visible, and they can be attributed to the deformation vibration of Fe-O bond presence of Fe$_3$O$_4$. At high carbonization temperatures (900 and 1000°C), the presence of C=O and C-O stretching vibrations is observed at the 1704 and 1089 cm^{-1}, respectively. XRD patterns of the samples are also shown in Fig. 2. A broad peak at 2-Theta = 10-30° in all samples corresponds to amorphous carbon. No sharp diffraction peak at 26–27° was observed in XRD patterns of both AC and 800-Fe(NO$_3$)$_3$ samples, indicating that no graphitic carbon is formed at 800°C. The diffraction peaks of catalytic 800-Fe(NO$_3$)$_3$ sample, however, match well with the (220), (311), (400), (422), (511) and (440) reflections of the standard phase of magnetite (Fe$_3$O$_4$).
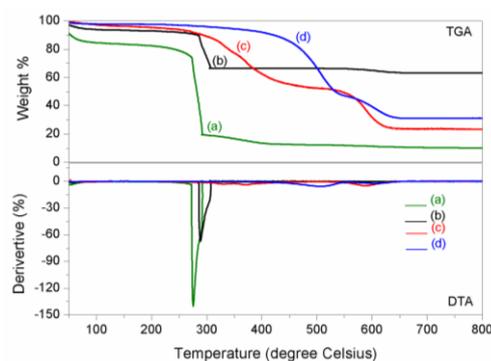

Fig. 1. TGA/DTA graphs of (a) AC, (b) 800-Fe(NO$_3$)$_3$, (c) 900-Fe(NO$_3$)$_3$ and (d) 1000-Fe(NO$_3$)$_3$.
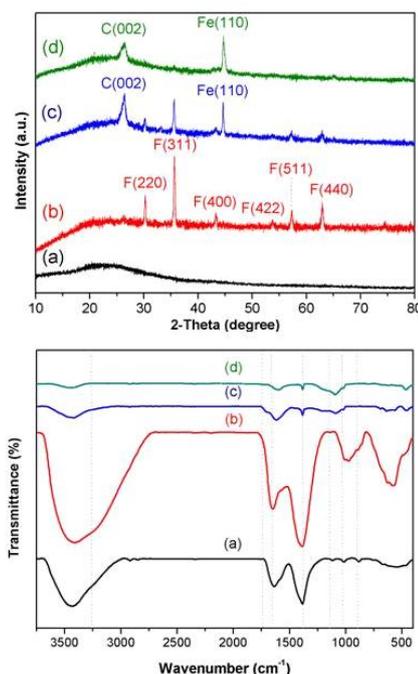

Fig. 2. FTIR and XRD spectra of (a) AC, (b) 800-Fe(NO$_3$)$_3$, (c) 900-Fe(NO$_3$)$_3$ and (d) 1000-Fe(NO$_3$)$_3$.

At 900°C, the relative intensity of Fe_3O_4 peaks is decreased. However, the sample exhibits the predominant peaks at 2-Theta = 26.40°, which can be attributed to the (002) reflection of graphitic carbon. The d_{002} values derived from this XRD pattern is slightly higher than that of the perfect graphite with d_{002} of 3.354 Å, indicating the multi-walled structure. Beside graphitic carbon and Fe_3O_4, the pattern also indicates the presence of Fe phase, which supports the growing mechanism of CNTs on metallic catalysts, as reported previously. This result confirms that Fe nanoparticles are important to promote the growth of graphitic carbon nanostructures in this study. At 1000°C, all of Fe_3O_4 is reduced to Fe nanoparticles, but less amount of graphitic carbon is observed in this sample. This might be due to the fact that the growth of carbon nanotubes is inhibited by that of Fe nanoparticles. The average crystallite size of the Fe crystals, calculated by Scherrer's equation at the most prominent (110) peak, is about 44 nm and 22 nm at 900°C and 1000°C, respectively.

Figs. 3a-3c present typical SEM images of the catalytic samples, which contains a significant amount of amorphous carbon, metallic catalyst, and graphitic carbon. Metallic catalyst in various forms (i.e., Fe, Fe_3O_4) can be well-defined displayed using BEI mode. Information about the shape and size of graphitic carbon, however, cannot be seen in the images. TEM images are then used to gain such information. From the figure (Fig. 3d), no graphitic carbon was found when pyrolyzing and carbonizing at 800°C. The appearance of graphitic nanocarbon with ring and shell geometries as well as Fe nanoparticles is detected for the carbonization at higher temperatures, i.e., 900-1000°C, as shown in Fig. 3e-3f. These ring geometry, instead of nanotubes, is typically reported to occur in graphitic nanocarbon with highly defective nanostructures [10].
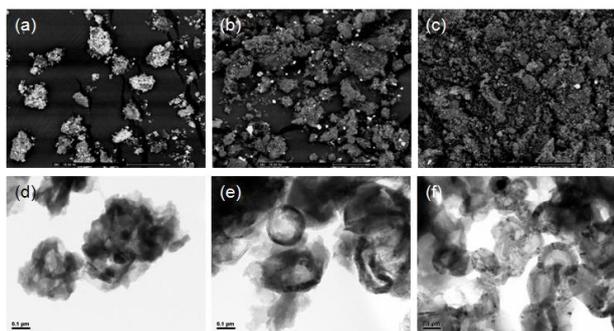

Fig. 3. TEM and SEM images of (a,d) 800-Fe(NO₃)₃, (b,e) 900-Fe(NO₃)₃ and (c,f) 1000-Fe(NO₃)₃.

The BET specific surface area, average pore diameter and total pore volume of samples are shown in Table 1. The results show that the agglomeration of Fe_3O_4 particles in Fig. 4c contributes to larger pore size and very small BET specific surface area. It is interesting that the maximum BET specific surface area of 1159 m^2/g with an average pore size of 3.9 nm is observed in 1000-Fe(NO₃)₃. This value is quite large when compared to 95.68 m^2/g of commercial carbon nanotubes [11] and that of activated carbon derived from sugarcane bagasse in this study (520 m^2/g).

Table 1. Specific surface area, total pore volume, and average pore size of samples.

Samples	BET specific surface area (m^2/g)	Total pore volume (cm^3/g)	Average pore size (nm)
AC	520	0.28	2.1
800-Fe(NO₃)₃	30	0.13	17.6
900-Fe(NO₃)₃	225	0.19	3.3
1000-Fe(NO₃)₃	1159	1.14	3.9

4. Conclusions

In conclusion, we demonstrate a technique to prepare graphitic carbon-based nanocomposites, using a low-cost carbon feedstock, i.e., sugarcane bagasse, and processes. This makes the method beneficial in term of industrial point of view and the product potentially useful in a wide range of applications such as photocatalysts and adsorbents. The graphitic carbon obtained in this study has unique ring and shell geometries. The specific surface area greater than 1000 m^2/g of the nanocomposites was achieved in this study. The results also confirm the dependence of graphic carbon/carbon nanotube production on the incorporation of transitional metal catalyst.

Acknowledgements

References

[1] H. W. Kroto, J. R. Heath, S. C. O'Brien, R. F. Curl, Nature **318**, 162 (1985).

[2] S. Iijima, Nature **354**, 56 (1991).

[3] T. W. Ebbesen, H. J. Lezee, H. Hiura, J. W. Bennett, H. F. Ghaemi, T. Thio, Nature **382**, 54 (1996).

[4] K. Hata, D. Futaba, K. Mizuno, T. Namai, M. Yumura, S. Iijima, Science **306**, 1362 (2004).

[5] B. Zheng, C. Lu, G. Gu, A. Makarovski, G. Finkelstein, J. Liu, Nano Letters **2**, 895 (2002).

[6] L. Dong, J. Jiao, S. Foxley, D. W. Tuggle, C. L. Mosher, G. H. Grathoff, Journal of Nanoscience and Nanotechnology **2**, 155 (2002).

[7] C. Chen, J. Hu, D. Shao, J. Li, X. Wang, Journal of Hazardous Materials **164**, 923 (2009).

[8] M. Torabi, S. K. Sadrnezhaad, Current Applied Physics **10**, 72 (2010).

[9] S. Qu, J. Wang, J. Kong, P. Yang, G. Chen, Talanta **71**, 1096 (2007).

[10] J. C. Charlier, Accounts of Chemical Research **35**, 1063 (2002).

[11] S. H. Hsieh, J. J. Horng, Journal of University of Science and Technology Beijing **14**, 77 (2007).

_____
[*]Corresponding author: vorrada@gmail.com